Confocal profiling of grooves and ridges with circular section using the divided aperture technique

J.F. Aguilar
Instituto Nacional de Astrofísica Óptica y Electrónica, Luis Enrique Erro No. 1, Sta. Ma. Tonantzintla, Puebla 72840, Pue., México

Recibido el 1 de marzo de 2005; aceptado el 25 de mayo de 2005

The divided-pupil technique for the simulation of confocal imaging is applied to remove those artifacts appearing due to the symmetry of the object. A rigorous treatment is used to model the imaging system which is a two-dimensional confocal microscope, working in reflection mode. Since the geometry of the associated electromagnetic problem is 2-D, the objects analyzed are highly symmetric and cylindrical. The advantages and limitations of this technique are discussed and shown by means of examples.

Keywords: Confocal microscopy; light scattering; optical profilometry.

La técnica de pupila dividida se aplica en la simulación de un sistema confocal formador de imágenes para eliminar elementos espurios debidos a la simetría del objeto. Un tratamiento riguroso es usado para modelar la formación de imágenes en el sistema el cual es un microscopio confocal en dos dimensiones; los objetos analizados son altamente simétricos y cilíndricos. Las ventajas y limitaciones de esta técnica son discutidas y demostradas por medio de ejemplos.

Descriptores: Microscopía confocal; esparcimiento de luz; perfilometría óptica.

PACS: 42.25.Fx; 42.30.Va

1. Introduction

One of the most important properties of the confocal scanning optical microscope is the "depth discrimination property" [1], which allows the device to perform as a surface profiler, [2, 4]. However the conventional treatment used in modeling the image formation in confocal microscopy is inadequate to obtain surface profile reconstructions with a high degree of confidence [5].

The application of rigorous treatments has revealed some of the limitations in the confocal profiling process [5]. Theoretical treatments predict erroneous results when large values of the local slope or the local curvature are present in the surface of the analyzed object [6]. Different kinds of limitations are those due to the symmetry of the profile itself. For example, when the surface of the object has a spherical shape, concave or convex, a maximum of intensity is expected when the confocal microscope is focused on the surface of the sphere. However, at least from the point of view of geometrical optics, another maximum value must appear when the microscope is focused on the center of the sphere. This could represent a problem when the confocal microscope is used as a profilometer. In fact, Weise *et al.* [7] have shown experimentally that when confocal scanning is performed along the axial direction passing through the center of a sphere, two maxima appear in the confocal signal, one corresponding to the position of the surface of the sphere and other with the center. Aguilar *et al.* [8] have also detected these two local maxima of intensity experimentally in confocal images of a steel ball; in the same work, the possibility of isolating these two maxima was discussed. In this case isolation was obtained using a stop to block one half of the pupil during the illumination and then blocking one half of the aperture of detection. This is known as divided-aperture imaging. The maximum of intensity associated with the surface may be selected when the light reflected along the backscattering direction is blocked and only the specular reflected light reaches the detector. This particular case of the divided pupil technique is known as the confocal stereoscopic configuration. Alternatively, when the opposite half of the aperture on the detection side is blocked, the light reaching the detector in the backscattering direction is admitted and the specular is blocked. In this case a maximum of intensity appears when the focus of the system coincides with the center of symmetry of the object being studied. This is essentially a dark field configuration.

The technique of the divided pupil has also been used for other applications, for example in ophthalmology, [9, 10]. Sheppard and Hamilton [11] have used the half stop for stereoscopic imaging, and Török *et al.* [12,13] have used both stereoscopic imaging and dark field configurations in confocal imaging.

The present work is based on the simulation of a two-dimensional confocal scanning microscope working in the reflection mode to perform surface profiling. A divided pupil is applied in order to remove the artifacts which appear when objects with spherical symmetry are imaged. A rigorous theory is used to describe the interaction of the wavefront with the object, and the boundary conditions of the electromagnetic problem associated with the imaging process are solved by a numerical technique. In a previous work [8], rigorous theory was also used but was restricted to the scalar approximation. Perhaps the main limitation of the simulation presented here is the restriction to a 2-D geometry, hence importantly the objects studied are ridges and grooves with a circular transversal section.

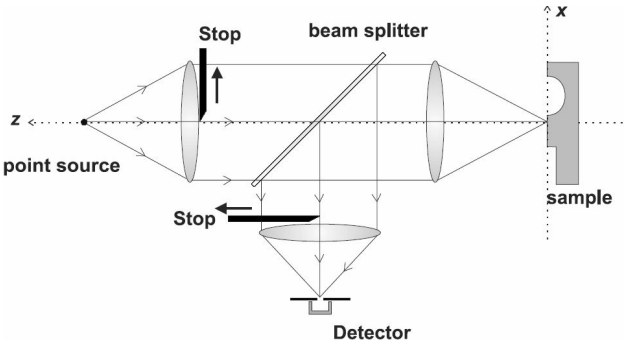

FIGURE 1. The optical system. This is a 2-D confocal microscope working in reflection mode. Stops blocking one half of the pupil in illumination and detection determine the configuration as stereoscopic imaging or dark field imaging.

2. The optical system and the illumination beam

The optical system considered here is depicted in Fig. 1, representing a confocal microscope in two dimensions. Keeping in mind this restriction, when a point source is referred to, it must be considered as a line source. Also, a lens must be understood as a cylindrical lens and a point detector is in fact a line detector. The objective lens forms an image of the point source on the $z = 0$ plane of the coordinate system. The sample is located in the focal region, and the light reflected from the object passes through the lens again and is then deflected by means of the beam-splitter; finally the tube lens concentrates the light on the detector. The stops are included to block one half of the illuminating beam and one half of the reflected beam reaching the detector, and they can be removed to restore the standard confocal configuration.

The 2-D confocal image is formed when the object is scanned in the z direction for each position in the x direction. An intensity value is associated with each pair of coordinates (x, z). This intensity function then represents the confocal image. In the simulation, it is necessary to calculate the electromagnetic field illuminating the object which will be referred to as the incident field $E_i(x, z)$. Because the profile of the sample has non-uniform height, some parts of the surface will be out of focus, and an expression for the incident field at each point $(x, \zeta(x))$ should be found. Here, $\zeta(x)$ is the function defining the surface profile of the the object. This expression has been derived using an angular spectrum technique. The incident field at the focal plane is assumed to be known, namely $E_i(x, 0) = sinc(2\alpha_m x/\lambda)$, where α_m is the numerical aperture of the system and λ is the selected wavelength. Although this expression is obtained from a paraxial approximation, it can be extended if the incident field as a function of the position (x, z) is written in the integral form

$$E_i(x,z)=\frac{1}{2\alpha_m}\int_{-\alpha_m}^{\alpha_m}(1-\alpha^2)^{1/4}e^{-ikz\sqrt{1-\alpha^2}}e^{ik\alpha x}d\alpha, \quad (1)$$

where k is the wave number $2\pi/\lambda$, and the factor $(1-\alpha^2)^{1/4}$ is an apodization function which is included to compensate for the distribution of energy in the pupil, and becomes important when high numerical apertures are considered. [14, 15].

In terms of optical coordinates u and v, Eq. (1) can be written as

$$E_i(v,u)=\frac{1}{2}\int_{-1}^{1}\left[1-(\alpha_m t)^2\right]^{\frac{1}{4}}e^{-i\frac{u}{\alpha_m^2}\sqrt{1-(\alpha_m t)^2}}e^{ivt}dt, \quad (2)$$

where $v = k\alpha_m x$ and $u = k\alpha_m^2 z$ [16]. This is the expression used for the numerical work and allows us to consider systems with high numerical apertures, say $N.A. > 0.6$.

3. Illumination with the divided pupil

Figure (2a) shows the intensity distribution at the focal region with the pupil totally open for a system with a Numerical Aperture of 0.9. Figure (2b) shows the intensity distribution corresponding to the incident field of the same system, but with one half of the pupil blocked. In these contour plots, which show the isophotes of the illuminating beam, it is possible to observe that, due to diffraction effects, some waves invade the dark half of the illumination cone, which is indicated by the dotted lines delimiting the geometrical shadow. Another important thing to take into consideration is the fact that, in the case of the divided pupil the illuminating beam is not symmetrical with respect to the optical axis. This could be drawback to this approach. However, as will be shown, the technique is very useful for distinguishing the effects arising exclusively from the circular symmetry.

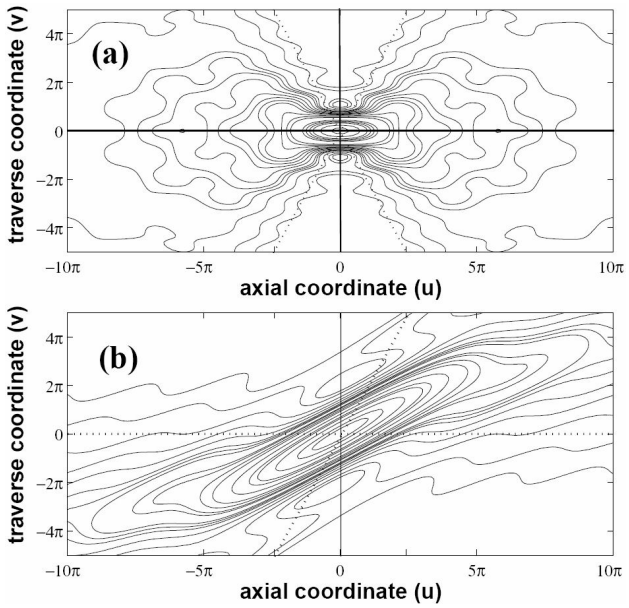

FIGURE 2. Isophotes representing the intensity distribution in the focal region of the system with a N.A. of 0.9. (a) when the pupil is totally open and, (b)when the pupil is half blocked.

4. Calculation of the confocal image

In a problem with cylindrical geometry such as that one considered here, it is well known that the vectorial character of the associated electromagnetic problem can be reduced to a scalar one. This can be done by separating the polarization into two independent cases: s polarization when the electric field vector is in the direction perpendicular to the plane of incidence (xz plane), and p polarization for the case with the electric field vector in the direction parallel to the plane of incidence. In the first case, only the magnitude of the electric vector is considered, while in the second, only the magnitude of the magnetic vector is taken into account. In both cases the resultant problem has a scalar character, but a complete vectorial treatment can be achieved by solving the problem for each polarization and then forming the vectorial sum of the components.

For simplicity's sake, only the solution of the scattering problem for the case of s polarization and objects made of a perfectly conducting material is presented here. This is a good approximation to the behavior of metallic objects with high reflectance such as those made of gold, aluminum or silver, for example. However some effects in the imaging process due to the finite conductivity could be a motive for concern, such as the excitation of surface plasmons, though they are beyond the scope of this paper.

Although different rigorous treatments exist for the problem of scattering and diffraction by a perfectly conducting cylinder [17,18], here the treatment developed by Maradudin *et al.* is used [19]. This has already been applied to image formation in the microscope and is most appropriate for the problem stated in this work. In fact, it can be extended for real materials, both conductor and dielectric, or for combinations of the two [20,21].

When an electromagnetic wave is incident on an interface, the total electric field $E(x,z)$ can be expressed in the form of an integral equation

$$\mathbf{E}(x,z) = \mathbf{E}_i(x,z) - \frac{1}{4\pi}\int_{-\infty}^{\infty} \left[G(x,z;x',z')\mathbf{F}(x')\right]|_{z'=\zeta(x')}dx', \quad (3)$$

where the first term on the right hand side represents the incident field associated with the illuminating beam discussed in the previous section. The second term, that containing the integral, is called the scattered or reflected field. The function G is the Green function, and it can be be verified for this particular geometry that this is the Hankel function of order zero and of the first kind,

$$G(x,z;x',z') = i\pi H_0^{(1)}\left(k\left[(x-x')^2+(z-z')^2\right]^{1/2}\right). \quad (4)$$

The unknown function $\mathbf{F}$ is the "source function" and contains essentially the boundary conditions of the problem, which in this case is the normal derivative of the electric field evaluated at the interface characterized for the function ζ. This is

$$\mathbf{F}(x') = D_{n'}\mathbf{E}(x,z)|_{z=\zeta(x)}, \quad (5)$$

where D_n is the normal derivative operator defined as

$$D_n = \left[-\zeta'(x)\frac{\partial}{\partial x} + \frac{\partial}{\partial z}\right], \quad (6)$$

with $\zeta'(x)$ the slope of the plane tangent to the surface.

To solve the integral equation for the unknown source function $\mathbf{F}(x)$, Eq. (3) can be reduced if the total electric field is evaluated at points located on the interface. This can be done by a limit process, evaluating the field at points approaching the surface from the vacuum, so that for the limit $(x,z) \to [x_0, \zeta(x_0)]$ it is possible to write

$$\mathbf{E}_i(x_0) = \lim_{\eta\to 0}\int_{-\mathsf{L}/2}^{\mathsf{L}/2} L_0(x_0;x',\eta)\mathbf{F}(x')dx', \quad (7)$$

where L represents the length of the surface and

$$L_0(x_0;x') = \frac{i}{4}H_0^{(1)} \times(k[(x_0-x')^2 + (\zeta(x_0+\eta-\zeta(x'))^2]^{1/2}), \quad (8)$$

with $\eta > 0$.

Repeating this approach for, say N pairs of coordinates $(x_m, \zeta(x_m))$ with $m = 1,2,\ldots,N$, and also discretizing the integral by dividing the interval of integration into N subintervals of length Δx, Eq. (7) can be converted into a matrix form which can be solved by means of conventional numerical methods. Once the matrix equation is solved for the boundary condition F, the expression for the scattered field is simplified by means of the asymptotic expansion for large arguments of the Hankel function. Finally, the scattered field is obtained as a function of the scattering angle θ and can be written as follows:

$$E_s(\theta) = -\Delta x\sum_{n=1}^{N} F_n \exp\left[-ik\left(x_n\sin\theta + \zeta(x_n)\cos\theta\right)\right]. \quad (9)$$

The confocal image is then determined by the integration of the amplitude of the scattered field over the whole angular range $[-\alpha_m : \alpha_m]$ of the pupil and then taking the modulus squared [22]. At this point, one can decide if one half of the pupil is blocked; in this case, integration is only over half of the range $[-\alpha_m : 0]$ or $[0 : \alpha_m]$, which, in combination with divided pupil illumination, determines the mode of image formation, either dark-field mode or stereoscopic mode.

5. Results and Discussion

For the simulated optical system, a numerical aperture of 0.9 and a wavelength of $0.632\mu m$ were selected. Results obtained with the technique of the divided pupil in stereoscopic

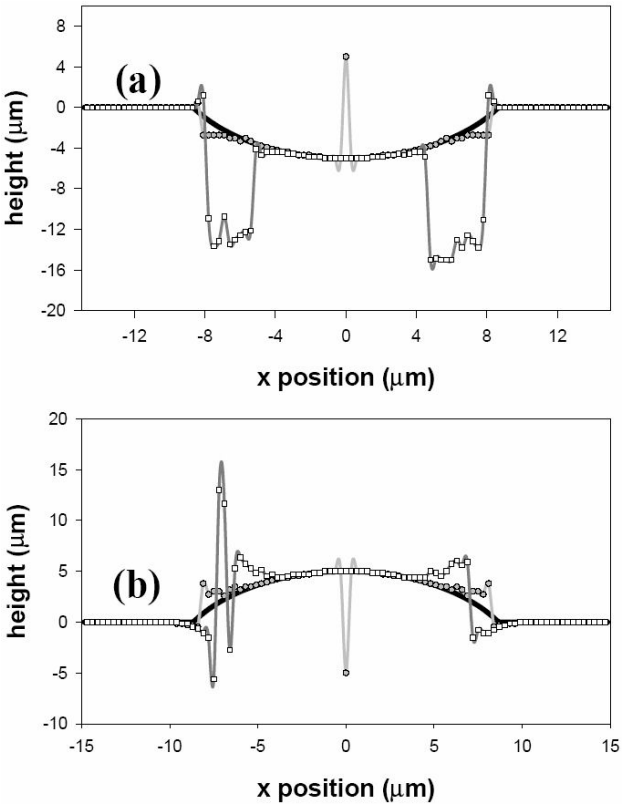

FIGURE 3. (a) The profile of a groove (solid thick line) of a circular section 20 μm in diameter. The profile retrieved with the normal confocal profiler is represented by the filled circles, and that obtained with the divided pupil in the stereoscopic configuration is represented with the empty squares. Figure 3b shows the transversal section of a ridge of the same dimensions and the retrieved profiles are represented in the same manner.

mode are presented in this section. The analyzed objects are in general grooves and ridges with a circular section, made on a flat substrate. The depth or the height of these structures is not necessarily equal to the radius of the circular transversal section, but vary in order to show that the maximum appears exactly at the center of symmetry. Figure 3 shows the profile of a groove (Fig. 3a) of circular section 20 μm in diameter. In the same figure, the retrieved profile with the standard confocal profiler is represented by the filled circles and that obtained with the divided pupil in the stereoscopic configuration is represented with the empty squares. Figure 3b shows the transversal section of a ridge of the same diameter as in 3a, and the retrieved profiles are represented in the same way. It can be noted that the retrieved profile with the standard confocal mode is quite accurate except at the point of high symmetry, which is at the center of the circle. This point can be removed with the divided pupil technique in stereoscopic mode, but additional mismatched points appear due to the asymmetry of the illuminating beam. However, better and more complete information is obtained from the full 2-D confocal images, which are presented in Figs. 4 and 5 for the standard confocal and stereoscopic confocal images respectively. Figure 4a shows the confocal image of the

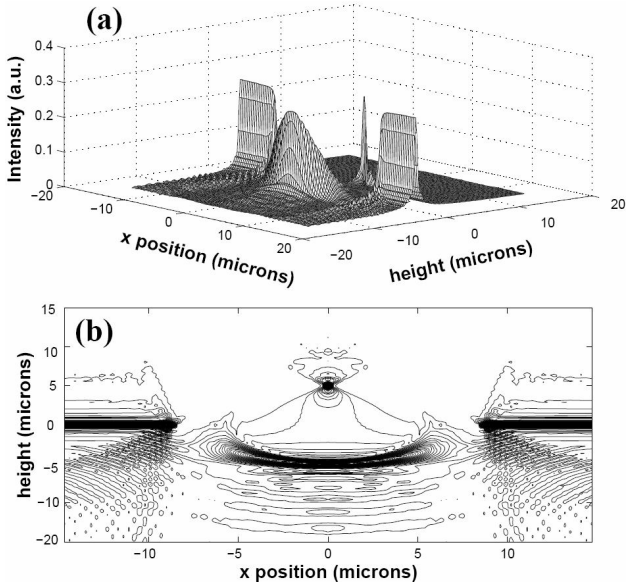

FIGURE 4. The whole confocal image of a groove. (a) shows the confocal image plotted in 3 dimensions, (b) contour curves of the image. Darker zones correspond to higher intensity regions of the image.

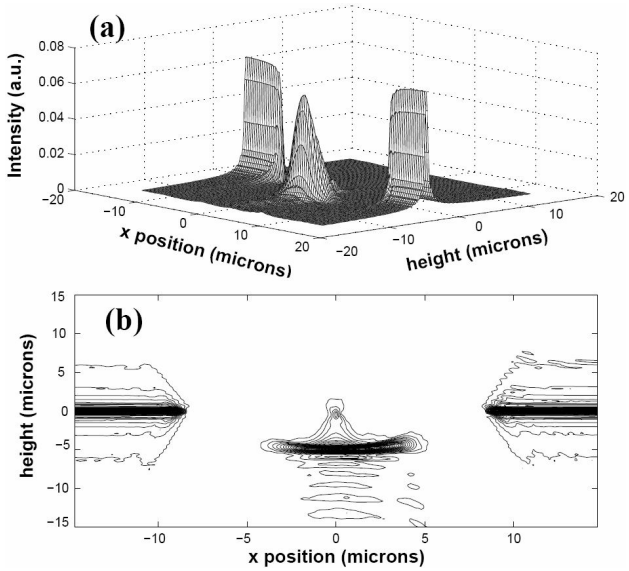

FIGURE 5. The stereoscopic configuration gives an image where only the real parts of the object are enhanced as is shown in Fig. 5a. Figure 5b also presents the enhanced intensity corresponding only to the profile of the object.

groove plotted in 3 dimensions, where one can easily appreciate the profile of the groove but also observe a peak of very high intensity. This is of course an artifact due to the circular symmetry of the object of the circular section. The effect is also evident in the corresponding contour curves of the image, since it is located at the geometric center appearing in Fig. 4b. Here the darker zones correspond to higher intensity regions of the image. The confocal stereoscopic configuration, on the other hand, gives an image where only the real

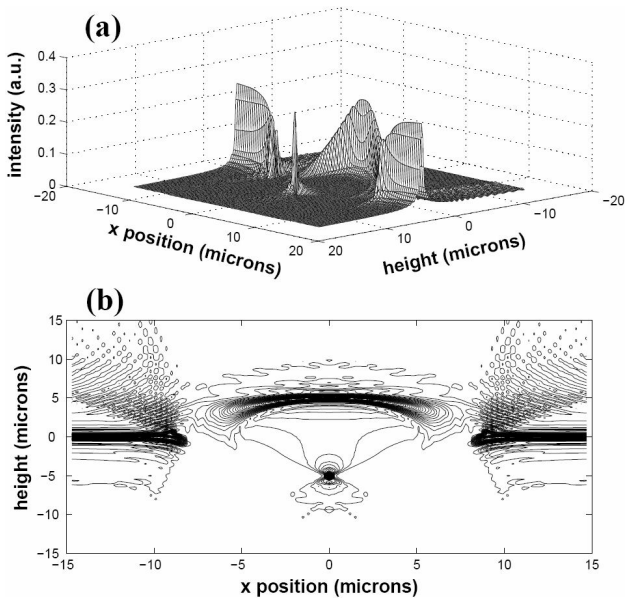

FIGURE 6. (a) The confocal image of a ridge of circular section 20 μm in diameter. (b) The contour curves of the image.

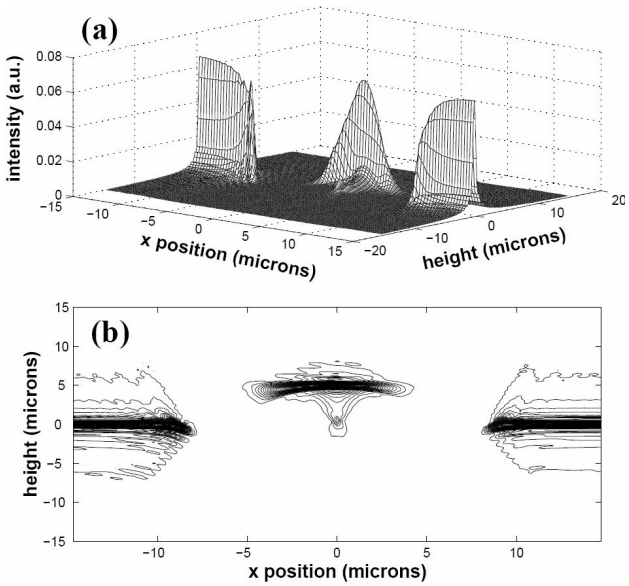

FIGURE 7. (a) The confocal image of the ridge $20\mu m$ in diameter obtained with the divided pupil in stereoscopic mode. (b) The contour curves of the image.

profile of the object results in high intensity, as is shown in Fig. 5a. The central peak has now disappeared and no artifacts are present. The contour curves shown in Fig. 5b also clearly show the aforementioned characteristics.

Figure 6 shows the confocal image of a ridge with a circular section 20 μm in diameter. Again the peak appearing at the axis of the cylinder has a height almost the same as that in the profile, as can be seen in Fig. 6a and in the contour curves of Fig. 6b. The image obtained with the divided pupil in the confocal stereoscopic mode is shown in Fig. 7; the central peak is no longer present, however a slight tilt can be noted in the contour curves of the image presented in Fig. 7b. This

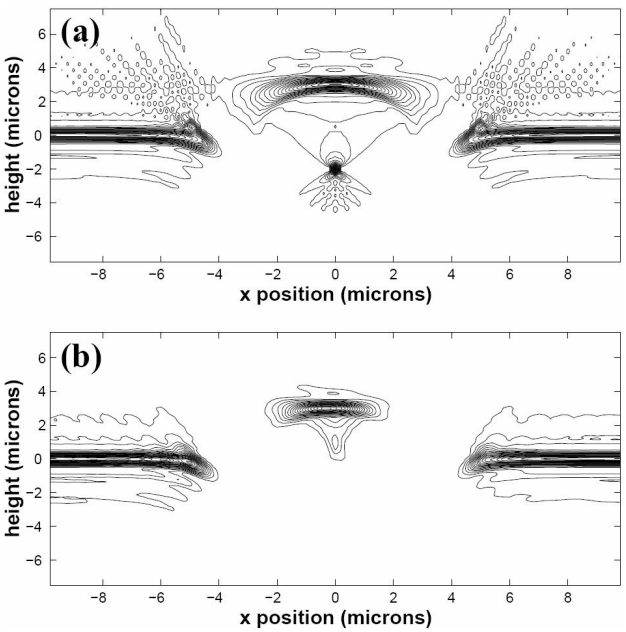

FIGURE 8. The contour curves of a ridge 5 μm in diameter as imaged, first with the confocal standard microscope (a), and then with the stereoscopic configuration (b).

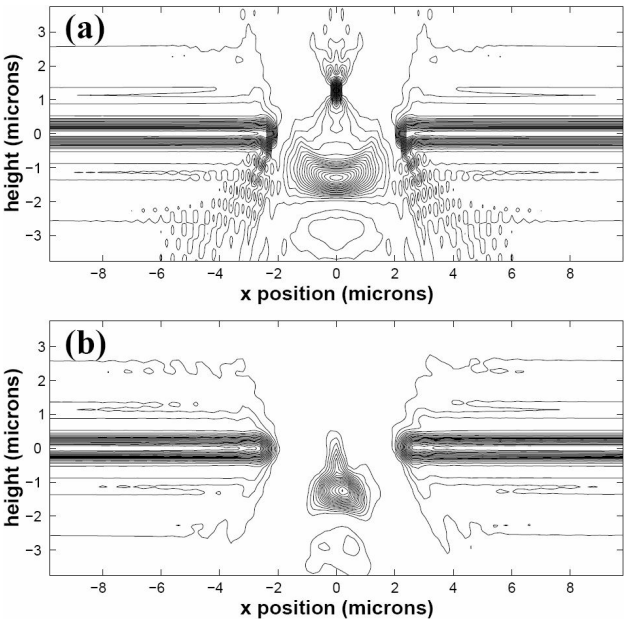

FIGURE 9. The contour curves of the image with the standard confocal (a) and stereoscopic (b) images of a circular groove 3 μm in diameter.

is because of the bias produced by the stop introduced at the pupil of the illuminating beam.

Another example is presented in Fig. 8, showing the contour curves of a ridge 10 μm in diameter, first with the confocal standard microscope (Fig. 8a) and then with the confocal stereoscopic configuration (Fig. 8b). Figure 9 presents the contour curves of the confocal standard and confocal stereoscopic images of a circular groove 5 μm in diameter. It is

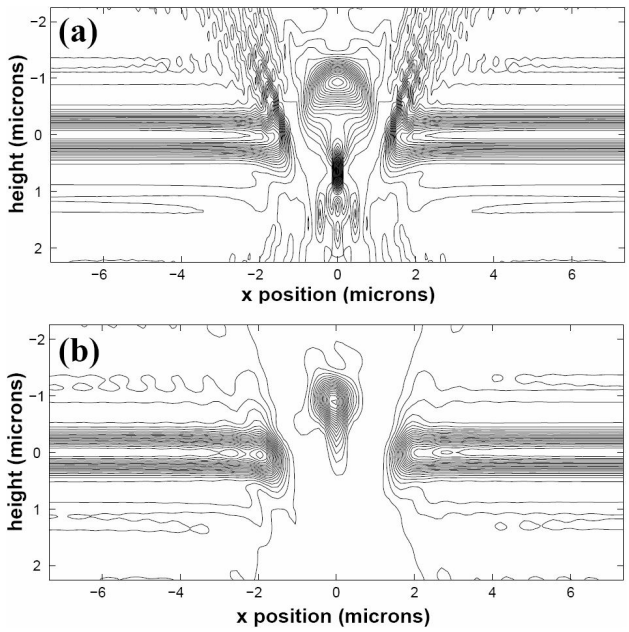

FIGURE 10. Images corresponding to a ridge 3 μm in diameter show the same effects but they are not so intense as in the case of the groove.

interesting to see the diffraction effects due to the small size of the details in the object. It is also easier to appreciate the artifact and the distortion in the case of the image with the stereoscopic mode. This is because of the multiple scattering effects due to the geometry of the object. In this case, the groove behaves like a cavity so that the light hits the wall of the sample several times before returning to the aperture of the objective lens. The mathematical approach used in this work takes this phenomenon into account, whereas it is usually neglected in conventional treatments of imaging. In Fig. 10, images corresponding to a ridge 3 μm in diameter show the same effects but they are not so intense as in the case of the groove.

6. Conclusion

In conclusion, a rigorous treatment of the light scattering phenomenon has been applied to the imaging process in a confocal system with the divided aperture, in two dimensions. The simulation of profiling cylindrical circular structures, such as grooves or ridges, shows the advantage of using this technique since some artifacts in the retrieved profile can be removed. The application of a rigorous treatment exhibits some effects that can not be seen when conventional techniques are used. It may also be concluded that the comparison of two images (normal confocal and stereoscopic confocal) can help to discriminate the artifacts from the real profile of the object.

Acknowledgment

This work has been supported by CONACyT through the project 37654-E.

1. D.K. Hamilton, *Opt. Lett.* **6** (1981) 625.
2. D.K. Hamilton and T. Wilson, *Appl. Phys. B* **27** (1982) 211.
3. C.J.R. Sheppard, T.J. Connolly, and M. Gu, *J. Mod. Opt.* **40** (1995) 2407.
4. C.J.R. Sheppard, A.R. Carlini, and H.J. Matthews, *Optik* **80** (1988) 91.
5. J.T. Sheridan and C.J.R. Sheppard, *Opt. Commun.* **105** (1994) 367.
6. J.F. Aguilar and E.R. Méndez, *J. Mod. Opt.* **42** (1995) 1785.
7. W. Weise, P. Zinin, T. Wilson, A. Briggs, and S. Boseck, *Opt. Lett.* **21** (1996) 1800.
8. J.F. Aguilar, M. Lera, and C.J.R. Sheppard, *Appl. Opt.* **39** (2000) 4621.
9. D.M. Maurice, *Experientia* **15** (1968) 1094.
10. C.J. Koester, *Appl. Opt.* **19** (1980) 1749.
11. C.J.R. Sheppard and D.K. Hamilton, *Appl. Opt.* **22** (1983) 886.
12. P. Török, C.J.R. Sheppard, and Z. Laczik, *Optik* **103** (1996) 101.
13. P. Török, Z. Laczik, and C.J.R. Sheppard, *Appl. Opt.* **35** (1996) 6732.
14. C.J.R. Sheppard and H.J. Matthews, *J. Opt. Soc. Am. A* **4** (1987) 1354.
15. B. Richards and E. Wolf, *Proc. Roy. Soc. A* **253** (1979) 358.
16. M. Born and E. Wolf, *Principles of Optics* 6^{th} Ed. (Pergamon, Oxford, 1980).
17. K.K. Miei and J.G. Van Bladel, *IEEE Trans. Antennas. Propag.* **AP-11** (1963) 185.
18. C.H. Papas, *J. Appl. Phys.* **21** (1950) 318.
19. A.A. Maradudin, T. Michel, A.R. McGurn, and E.R. Méndez, *Ann. Phys.* **203** (1990) 209.
20. J. Felix Aguilar and E.R. Mendez, *Proc. SPIE* **1926** (1993) 18.
21. J. Felix Aguilar and E.R. Mendez, *J. Opt. Tech.* **69** (2002) 422.
22. T. Wilson and C.J.R. Sheppard, *Theory and Practice of Scanning Optical Microscopy* (Academic, London, 1984).